Highlights

An efficient chemistry-enhanced CFD model for the investigation of the rate-limiting mechanisms in industrial Chemical Vapor Deposition reactors

Paris Papavasileiou, Eleni D. Koronaki, Gabriele Pozzetti, Martin Kathrein, Christoph Czettl, Andreas G. Boudouvis, T.J. Mountziaris, Stéphane P.A. Bordas

- An efficient CFD model is proposed for an industrial CVD reactor
- A reduced chemistry model for the deposition of alumina is proposed
- Coating thickness is predicted (5% error) in various positions inside the reactor
- The balance between chemical kinetics and diffusion is studied with the CFD model
- Results suggest that the process is in the reaction kinetics limited regime

An efficient chemistry-enhanced CFD model for the investigation of the rate-limiting mechanisms in industrial Chemical Vapor Deposition reactors

Paris Papavasileiou[a,b], Eleni D. Koronaki[a,b,*], Gabriele Pozzetti[c], Martin Kathrein[c], Christoph Czettl[d], Andreas G. Boudouvis[b], T.J. Mountziaris[e], Stéphane P.A. Bordas[a,b]

[a] *Faculty of Science, Technology and Medicine, University of Luxembourg, Maison du Nombre, 6 Avenue de la Fonte, Esch-sur-Alzette, L-4364, Luxembourg*
[b] *School of Chemical Engineering, National Technical University of Athens, 9 Heroon Polytechniou str., Zographos Campus, 15780, Attiki, Greece*
[c] *CERATIZIT Luxembourg S.à r.l, Mamer, L-8201, Luxembourg*
[d] *CERATIZIT Austria GmbH, Reutte, A-6600, Austria*
[e] *William A. Brookshire Department of Chemical & Biomolecular Engineering, University of Houston, Houston, TX, USA*

Abstract

An efficient CFD model for the deposition of alumina from a gas mixture consisting of $AlCl_3$, CO_2, HCl, H_2 and H_2S in an industrial CVD reactor with multiple disks and a rotating feeding tube, is proposed. The goal is twofold: (i) to predict the thickness of the deposited material, (ii) to investigate whether the process rate is determined by the reaction rate or by diffusion. A reaction model that consists of a gas-phase homogeneous reaction and a heterogeneous reaction is implemented, with a proposed kinetics rate that includes the effect of the H_2S concentration. The latter has a catalytic effect, but the mechanism is not entirely understood. The entire reactor geometry (consisting of 40-50 perforated disks) is divided into appropriately chosen 7-disk sections. The 2D, time-dependent CFD model is

[*] Corresponding author
Email address: ekor@mail.ntua.gr (Eleni D. Koronaki)

validated using production data for the deposition thickness. The proposed computational tool delivers accurate predictions (average relative error 5%) for different geometries corresponding to real reactor set-ups. Extending the functionality beyond prediction, a computational experiment is performed to illuminate the interplay between species diffusion and chemical reaction rates, which determines the rate-limiting mechanism. The results indicate that species diffusion is fast enough and therefore reaction kinetics determine the overall deposition rate.

Keywords: Chemical Vapor Deposition, Computational Fluid Dynamics, Industrial Reactor Modeling, α-Al_2O_3 deposition, Rate-limiting step

---

Published journal article available at:
https://doi.org/10.1016/j.cherd.2022.08.005

1. Introduction

Chemical Vapour Deposition (CVD), where a solid coating is deposited on a heated surface from a mixture of gas reactants is used for diverse applications, including: microelectronics (Creighton and Parmeter, 1993), polymers for microfluidics, sensors and membranes (Ozaydin-Ince et al., 2011) and wear resistant coatings (Kathrein et al., 2003; Gassner et al., 2019). It is a complex process involving competing physical phenomena, such as convection, diffusion and chemical reactions. The balance established between transport phenomena and chemistry is critical for determining the efficiency of the process and the quality of the produced material.

Computational Fluid Dynamics (CFD) models of CVD processes that account for the transport of mass, momentum and species inside reactors have been proposed in order to elucidate the interplay between the different

mechanisms and its effect on the process (Jensen et al., 1991; Theodoropoulos et al., 1997; van Santen et al., 2001; Cho and Mountziaris, 2013). Such models have also been used for optimizing the design of CVD reactors (Theodoropoulos et al., 2000; Yousefian and Pimputkar, 2021), as well as for predicting reaction rates inside the reactor (Barua and Povitsky, 2020). Zou et al. (2021) successfully tried to analyze industrial CVD reactors using a porous media approach. This approach was used in order to tackle the difficulty of explicitly modelling the large amount of substrates in the system by modelling the substrate-packed drawers of the reactor as porous media. Others have thoroughly investigated the reactant gas flow regimes inside of the reactors (Gkinis et al., 2017), as well as the effect of the flow on the produced coatings (Gakis et al., 2015; Cheimarios et al., 2019). Mitrovic et al. (2006a,b, 2007) in a series of publications, analyzed the flow inside a rotating disk reactor for different process parameters using CFD, determined the optimal parameters for the application and then optimized the reactor design by using the results of the simulations. Nevertheless, their work did not include a chemistry model and hence it was not possible to assess the effect of the flow on the deposited film.

Despite the progress in computer-aided analysis of CVD reactors, important challenges remain, especially in industrial-scale processes:

1. Industrial CVD reactors have a complex geometry in order to increase the coated surface and the throughput of the process. This translates into time-dependent models involving three-dimensional computational geometries, often with moving mesh and therefore, increased level of computational complexity and cost.
2. The actual network of gas-phase and heterogeneous reactions that ulti-

mately lead to deposition, are often not completely known. For example, in the chemical system studied here, the role of hydrogen sulphide is not entirely understood, although its positive effect of the deposition rate has been widely observed (Oshika et al., 1999; Blomqvist et al., 2011; Ruppi, 2020).

3. Even when there is a well-established chemical network, it often involves dozens of reactions and intermediate species. Integrating such a chemistry pathway in a CFD model, would make it computationally intractable. Moreover, even when the chemical system is known, ie. the specific reactions and their kinetic rates, the effective reaction rates have to be determined for the particular application and geometry.
4. The geometry of the reactor changes, even in a day-to-day basis in industrial practice. This is not true for every type of CFD application, but it is particularly true in the industry of cutting tools and wear resistant coatings. Therefore, it is important for the usability of the model to easily accommodate changes in the computational geometry in an almost automatic way.

Points 2 and 3 have been addressed in the past by developing reduced order models of CVD in conjunction with deposition chemistry models (Cheimarios et al., 2012; Gakis et al., 2015; Koronaki et al., 2016; Gkinis et al., 2017; Spencer et al., 2021). Nevertheless, these reduced order strategies require large amounts of data from detailed models which are often computationally intractable.

In this work we focus on addressing the combination of points 1, 2 and 3 in an industrial-scale CVD application and illustrate the implementation of an efficient modeling strategy that hinges CFD with an effective deposi-

tion model, validated by production data. The geometry of the investigated CVD reactor changes on a day-to-day basis, which is why addressing Point 4 is important and will be the subject of future work. Despite the simplifications of the CFD model, we present its potential not only as a predictive tool but also as a means of suggesting the dominance of reaction kinetics in terms of determining the rate-limiting steps of the process. This is an important contribution, because in the context of an industrial process, it is not always feasible to measure the deposition rate experimentally in different temperatures and produce an Arrhenius plot to map out the diffusion and reaction limited regimes.

The application addressed here, is the deposition of alumina onto three-dimensional cemented carbide cutting tools with a well-established thermal LP-CVD process from a gas mixture consisting of $AlCl_3$, CO_3, HCl, H_2 and H_2S (Hochauer et al., 2012) in a commercial reactor consisting of several perforated disks and a rotating inlet tube (Sucotec SCT600TH). Several other suggested CVD processes exist for the deposition of Al_2O_3, such as a MO-CVD process utilizing aluminium tri-isopropoxide (ATI) as a precursor (Etchepare et al., 2014) or a PE-CVD process utilizing dimethylaluminum isopropoxide (DMAI) as a precursor (Ban et al., 2017). These processes not only require a lower thermal budget, but also utilize a safer gaseous atmosphere. However, for our specific application (i.e. wear resistant coatings for cutting tools) and because of the targeted properties of the alumina coating, the aforementioned thermal LP-CVD process is used.

Alumina is very popular for wear-resistant coatings (Kathrein et al., 2003; Gassner et al., 2019) because of its properties (Gassner et al., 2018; Stylianou et al., 2019) and the improved chemical stability and high temperature hardness it provides in Al_2O_3/TiCN multilayer coatings (Quinto,

1996; Prengel et al., 1998; Paseuth et al., 2016). The effect of process conditions on the growth and texture of α-Al_2O_3 has been studied (Ruppi, 2020), since both directly influence the final properties of the α-Al_2O_3-coated cutting tools. However, little work has been done on the process of the CVD of hard coatings.

The following sections are structured as follows: The geometry and operation of the studied chemical vapor deposition reactor is presented in Section 2. The details of the developed CFD model are discussed in Section 3. Subsequently, the results of the CFD model are detailed in Section 4 along with an analysis of the rate-determining step of the process, followed by the conclusions in Section 5.

2. Chemical vapor deposition reactor geometry and operation

2.1. Reactor set-up and process conditions

This work focuses on the CVD of alumina on cutting tools, referred to henceforth in the text as inserts. An overview of the phenomena taking place inside a CVD reactor is presented in Figure 1. Inserts have various shapes and sizes (Fig. 2a) depending on their use in industrial applications but are invariably required to maintain cutting capacity for the prescribed time indicated by the manufacturer (Bar-Hen and Etsion, 2017). For this reason, the special coatings deposited, such as the alumina coating studied here, not only increase longevity but also ensure the expected usability of the insert.

The deposition of alumina on the inserts is studied in an commercial, industrial CVD reactor (Sucotec SCT600TH) which typically consists of 40-50 perforated disks, stacked one on top of the other shown in Fig. 2b. For

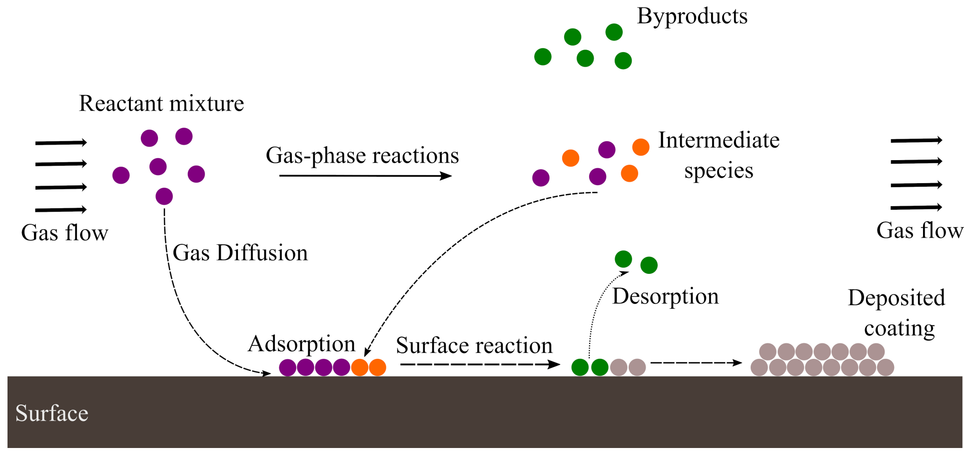

Figure 1: Overview of the interplaying mechanisms and phenomena of a CVD process.

reasons of clarity, a partial schematic of the reactor, depicting 3 disks is shown in Fig. 2c. The inserts are placed on the disks, as shown in Fig. 2d, while carefully designed perforations allow for the transport of the gas reactants between the disks and around the inserts. For each type of insert, there is a dedicated design of perforated disk, to accommodate the particular geometric characteristics. The mixture of gas reactants enters the reactor through a cylindrical tube at the center of the disk structure, through two inlet holes per disk, placed antipodally (shown in red in Fig. 2c). There is a 60° angle difference between the inlet holes of each disk-level of the reactor and the feeding tube rotates at a constant speed of 2 RPM. The gas mixture exits the reactor through holes in the perimeter of each disk (shown in blue in the schematic of Fig. 2c).

A two step coating process takes place inside the reactor (Stylianou et al., 2019). As a first step, a Ti(C,N) base layer of about 9 μm is grown on the cemented carbide cutting inserts. An α-Al_2O_3 layer is then deposited from $AlCl_3$–CO_2–HCl–H_2–H_2S at $T = 1005$°C and $P = 80$ mbar. The inlet gas

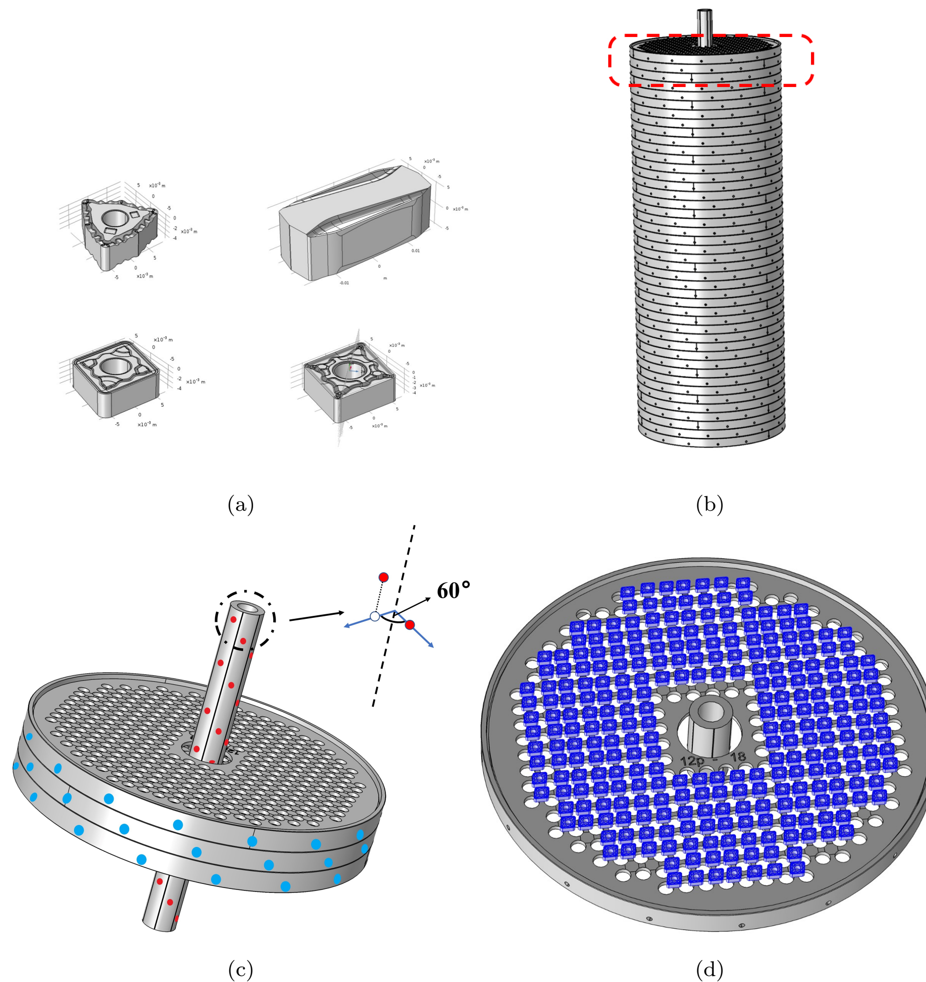

Figure 2: (a) Examples of the different cutting tool inserts that are coated inside the reactor. The shapes and sizes of the different inserts coated in the same reactor may differ significantly. (b) A 3D representation of the entire reactor. (b) A close up representation of a 3-disk part of the reactor. The rotating inlet tube passes through the center of the stack of disks. The gas reactants enter through the perforations shown in red. There are two holes per disk level, placed so that there is a 60° angle between the holes in neighbouring disks. The gas outlets are shown in blue. (d) An example of a perforated disk loaded with inserts. The inserts are shown in blue.

reactant volumetric fractions are 1.7% for $AlCl_3$, 3.7% for CO_2, 2.1% for HCl, 92.2% for H_2 and 0.3% for H_2S. The total inlet gas flow rate is 65 L/min ($P = 80$ mbar, $T = 1005$°C) (Hochauer et al., 2012).

2.2. Available production data

The production data available to validate the proposed model, are a total of 15 coating thickness measurements on inserts placed at selected locations inside the reactor, shown in Fig. 3.

For each production run, the coating thickness on the inserts at five disks are considered:

1. The top insert-containing disk of the reactor.
2. The 3rd or 4th disk from the top.
3. The middle disk.
4. The 3rd or 4th disk from the bottom.
5. The lowest insert-containing disk of the reactor.

On each of the aforementioned disks, there are and 3 positions of interest. Specifically:

1. The position closest to the inlet, R_0.
2. The position in the mid-distance between the inlet and the outlet, $R_{1/2}$.
3. The position closest to the outlet, R.

All measurements are in μm, with a precision of 0.1 μm.

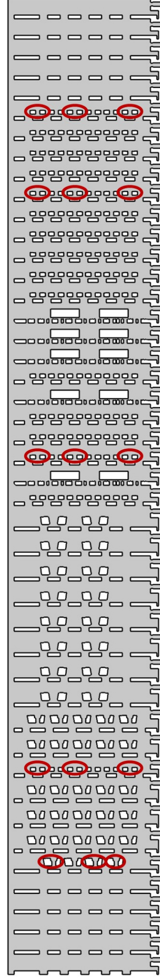

Figure 3: A 2D representation of the entire reactor indicating in red the 15 positions with available α-Al_2O_3 coating thickness measurements. The leftmost position is the one closest to the inlet.

3. Description of the CFD model

3.1. Governing equations

The governing equations include the conservation of mass and momentum, as well as the equations for the transport of chemical species and the

occurring chemical reactions. A detailed overview of the system of equations can be found in the publication of Gakis et al. (2015).

The reactor's operating temperature is considered constant in the entire domain. This is due to the fact that the entire reactor set-up is placed inside a furnace and therefore the entire system is heated up to a tightly controlled temperature of 1005°C. The ideal gas assumption is made for calculating the density of the gas mixture. The flow is considered laminar and incompressible. All calculations are made in transient conditions to account for the rotation of the gas inlet tube.

The equations were discretized with the finite element method and solved using COMSOL Multiphysics®. Linear basis functions are used for the continuity equation and quadratic functions for the rest. The computational geometry is presented in detail in the following paragraph.

3.2. Computational geometry

The reactor geometry is inherently non-axisymmetric and time-dependent due to the rotation of the vertical tube and the placement of the inlet holes. Therefore, a fully representative simulation would have to account for the entire 40-50 disks, in 3D, while also being time-dependent with a moving mesh. This, however, would come hand in hand with a significant computational cost, even when excluding the mass balances of the species that participate in the multitude of chemical reactions that will be discussed in detail in the following paragraph.

A two-dimensional computational geometry is proposed with appropriately selected boundary conditions. Furthermore, the computational domain does not include all the disks but rather accounts for parts of the reactor, containing 7 disks (cf. Fig. 4). The number of disks in the model is de-

termined by gradually decreasing the number of disks (from 11 to 7) and comparing the deposition thickness in the middle disk to the available production data. By gradually decreasing the number of disks considered, we are able to select the lowest number of disks for which the effects of the top and bottom boundary conditions do not affect the prediction of film thickness at the disk of interest (the middle disk). Another aspect that contributes to efficiency is linked to the fact that different reactor set ups may have several 7-disk parts in common. For example, an alternative reactor configuration could contain the same 7-disk sequence. In this fashion, it is possible to draw conclusions for several combinations of the 7-disk model, that would otherwise require the solution of new entire reactor models each time.

By using this 7-disk, two-dimensional approach and by simulating for 2 periods (or turning cycles) of the process, we can in turn average the deposition rates on each insert and obtain an equivalent deposition rate for several positions of interest inside the reactor.

3.3. Boundary conditions

To account for the rotating inlet tube, in the context of a two dimensional geometry, time-dependent inlet boundary conditions are applied. The perforations of the rotating tube, through which the gases are introduced into the reactor are represented by a fixed inlet boundary in the computational geometry in each disk level. The gas feed velocity is prescribed at each inlet as a time-dependent function that varies between 0 and V_{max} as a pulse that mirrors the rotation of the inlet tube. The maximum velocity value (V_{max}) is determined based on the experimental conditions and the geometry. Specifically, the following are taken into account:

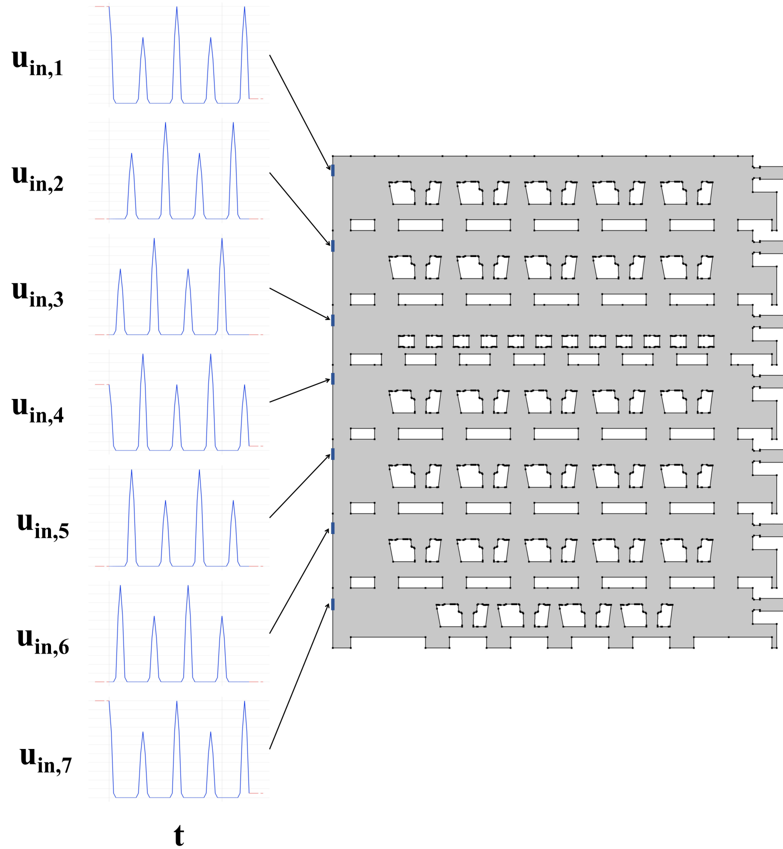

Figure 4: Inlets (highlighted in blue) and applied pulse boundary conditions for each one of them. The selected outlet boundaries are presented in red.

1. The inlet tube rotates with a rotational speed of 2 RPM.
2. The total inlet gas flow rate is 65 L/min ($P = 80$ mbar, $T = 1005$°C).
3. There is an average of 35 disks per run.
4. There are two perforations on the inlet tube for each disk. These two perforations are antipodal and their average diameter is 0.002 m.
5. There is a 60° angle difference between the perforations for each disk.

For the 7-disk geometry, the inlets along with the pulse boundary conditions

applied to them are shown in Fig. 4. It should also be noted that the chemical species' concentrations at the inlet are calculated using the volumetric percentages found in Section 2.1 and the species' molar fractions at the inlet are set to 0.0385 for CO_2, 0.0169 for $AlCl_3$, 0.0210 for HCl, 10^{-6} for H_2O and CO, 0.9203 for H_2 and 0.0033 for H_2S.

In order to reflect the actual geometry (cf. Fig. 2), where the outlet perforations are not aligned, the prescribed outlet pressure boundary conditions are applied at every other disk level. This means that out of the seven available outlets, only the first, the third, the fifth and the seventh from the top are considered open (marked in red in Fig. 4).

3.4. Chemistry model - Modeling the α-Al_2O_3 deposition

Several authors have studied the CVD of α-Al_2O_3 from a mixture of $AlCl_3$–CO_2–HCl–H_2–H_2S; for reasons of completeness, a brief overview is presented. The deposition appears to take place due to the hydrolysis of $AlCl_3$ in the presence of H_2O via the following surface reaction (Schierling et al., 1999; Catoire and Swihart, 2002; Ruppi, 2020):

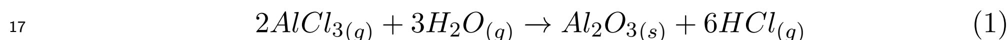

$$2AlCl_{3(g)} + 3H_2O_{(g)} \rightarrow Al_2O_{3(s)} + 6HCl_{(g)} \quad (1)$$

while H_2O is produced in situ in the gas phase via the water-gas shift volumetric reaction (Bustamante et al., 2004):

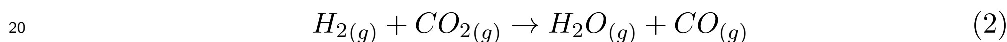

$$H_{2(g)} + CO_{2(g)} \rightarrow H_2O_{(g)} + CO_{(g)} \quad (2)$$

It must be noted, that this direction of the water gas shift reaction is endothermic (Keiski et al., 1996), however, due to the small amount of CO_2 in the gas-phase, we expect no changes in the isothermal profile of the reactor. Another assumption is that the consumption of precursor does not affect the flow, which is reasonable due to its low concentration in the gas phase.

Although the work of Catoire and Swihart (2002) highlights the complex mechanisms of the deposition kinetics, implementing this chemistry model that consists of 104 reactions and involves 35 species would inflate the computational cost of the CFD model. Given that the computational geometry is already a discounted representation of the actual reactor, it makes sense to implement the effective kinetics proposed in the work of Schierling et al. (1999). In their work, Schierling et al. (1999) propose a simple reaction scheme, consisting of four reactions with two possible intermediate species in the gas phase, namely $AlCl_2OH$ and AlOCl. The detailed suggested reaction mechanism is the following:

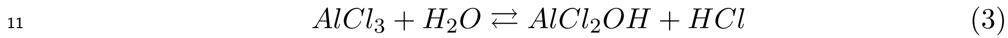

$$AlCl_3 + H_2O \rightleftarrows AlCl_2OH + HCl \tag{3}$$

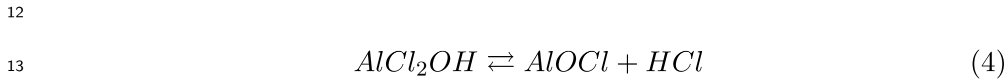

$$AlCl_2OH \rightleftarrows AlOCl + HCl \tag{4}$$

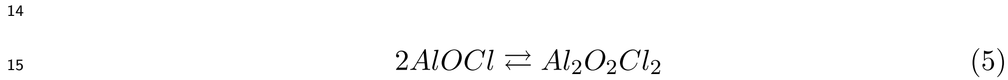

$$2AlOCl \rightleftarrows Al_2O_2Cl_2 \tag{5}$$

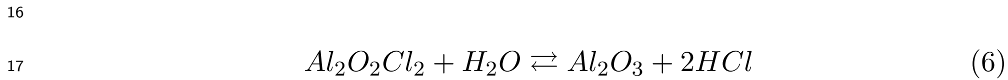

$$Al_2O_2Cl_2 + H_2O \rightleftarrows Al_2O_3 + 2HCl \tag{6}$$

According to the authors, the second step (eq. 4) is the rate-limiting reaction for the surface reaction, while the first step (eq. 3) is in the state of equilibrium. Based on this reaction mechanism, the first suggested deposition rate (R_{dep_1}, eq.7) is derived. The authors then proposed a second empirical rate (R_{dep_2}, eq.8) for an assumed parallel reaction path, with the aim of closely reproducing their experimental data. However, the rate remains empirical since the authors were not successful in searching for a second or third pos-

1 sible reaction sequence. Ultimately, the sum of these two deposition rates
2 $(R_{dep_1} + R_{dep_2})$ makes up the total α-Al_2O_3 deposition rate.

$$R_{dep_1} = k_1 \cdot p_{AlCl_3} \cdot p_{H_2O} \cdot p_{HCl}^{-1} \quad (mol \cdot m^{-2} \cdot s^{-1}) \tag{7}$$

$$R_{dep_2} = k_2 \cdot p_{AlCl_3}^{0.7} \cdot p_{CO_2}^{0.25} \cdot p_{H_2}^{0.2} \cdot p_{HCl}^{-1} \quad (mol \cdot m^{-2} \cdot s^{-1}) \tag{8}$$

where p_i denotes the partial pressure of each reactant i. The kinetic rate for the water gas shift reaction (eq.2) for a temperature of 1005°C is calculated through equation 9 (Tingey, 1966):

$$R_{wgs} = \frac{d[CO]}{dt} = k_{wgs} \cdot e^{-E_a/(RT)}[H_2]^{0.5}[CO_2] \quad (mol \cdot m^{-3} \cdot s^{-1}) \tag{9}$$

3 where units in brackets denote the concentration of each reactant in $mol \cdot$
4 m^{-3}, the pre-exponential factor (k_{wgs}) is equal to $1.2 \cdot 10^{16} m^{1.5} \cdot mol^{-0.5} \cdot s^{-1}$
5 and the activation energy (E_a) is equal to $326.36\ kJ \cdot mol^{-1}$.

6 The homogeneous water-gas shift reaction (eq. 2) takes place in the
7 domain of the simulation as indicated in Fig. 5a. Following experimental
8 evidence, α-Al_2O_3 deposition (eq. 1) is considered to take place on all in-
9 terior surfaces of the reactor, including the reactor walls, the inserts and
10 the disks on which the inserts are placed. The only surfaces excluded are
11 the reactor's inlets and outlets. A visual representation for the boundaries
12 selected for the deposition can be observed in Fig. 5a. The α-Al_2O_3 depo-
13 sition kinetic rate constants, k_1 (eq. 7) and k_2 (eq. 8) are fitted based on
14 production coating growth data. Due to the lack of production data for dif-
15 ferent reaction temperatures, it is not possible to fit both a pre-exponential
16 factor $(k_{0,i})$ and an activation energy $(E_{a,i})$ for each deposition rate. There-
17 fore, the entire deposition kinetic constants $(k_i = k_{0,i} exp(-E_{a,i}/RT))$ are

fitted all at once. For the WGS reaction, the pre-exponential factor is modified during fitting. However, no modification of the activation energy takes place.

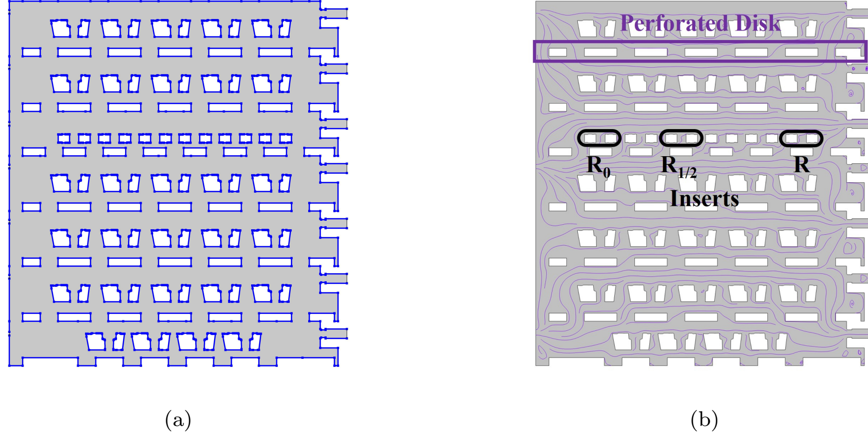

Figure 5: (a) Surfaces where α-Al_2O_3 deposition takes place are shown in purple; the volumetric Water Gas Shift reaction takes place in the area shown in gray. (b) Examples of the 2D representation of the inserts and perforated disks, in the computational domain.

Given the gas flow and reactant concentration profiles inside the reactor, the α-Al_2O_3 deposition (h_{dep}) for the entire production time is given by eq.10, integrating the deposition rates on the deposition boundaries for each insert of interest over the simulated $60s$ of the deposition process. The result of this integration is the deposition (in mol/m^2) that took place in the 60 simulated seconds (or 1 minute) of the process. By multiplying this result with the ratio of $(M_{Al_2O_3}/\rho_{Al_2O_3})$ we obtain the deposition thickness (in m) for the simulated $60s$ of the process. This result is then multiplied by the duration of the deposition process in minutes (t_{dep} - in this implementation, 3h), in order to calculate the deposition thickness for the entire process

duration.

$$h_{dep} = t_{dep} \frac{M_{Al_2O_3}}{\rho_{Al_2O_3}} \int_{0s}^{60s} (R_{dep_1} + R_{dep_2})\, dt \quad (m) \tag{10}$$

where $M_{Al_2O_3}$ and $\rho_{Al_2O_3}$ denote the molecular mass and density of the produced α-Al_2O_3 coating. The molecular mass of α-Al_2O_3 ($M_{Al_2O_3}$) is 101.96 g/mol and the value of density at 1005°C is taken from Munro (1997) and is equal to 3891 kg/m^3.

The implementation of the kinetic constants proposed in Tingey (1966) for the Water Gas Shift reaction, results on under-prediction of the overall coating deposition, attributed to low water availability. This motivated further investigation into the mechanisms that contribute to the in-situ production of water. Based on the more complex reaction scheme given by Catoire and Swihart (2002), the WGS reaction is not the only water-producing reaction. In fact, three different pathways (including the WGS reaction) are responsible for the production of water inside the reactor. All three pathways are able to form water in comparable amounts and are therefore considered competitive and coupled. The authors also suggest that the AlOCl intermediate plays a vital role in one of the aforementioned water production channels. In the publication of Tan et al. (2005), the effect of the AlOCl intermediate in water production is also acknowledged. However, the authors identified this effect as a catalytic effect on the Water Gas Shift reaction. Based on these previous findings the rate-constant of the Water Gas Shift reaction is fitted to capture the thickness measurements available in the production data.

Finally, Blomqvist et al. (2011) investigated the effect of H_2S in the deposition of alumina under a chemical system similar to the present one. Although the H_2S appears to have minimal to non-existent effect on the

Water Gas Shift reaction in the gas phase, the authors claim that H_2S as a true catalyst on the surface of α-Al_2O_3. However, the true mechanism of this effect is still obscure. For this reason, we also propose a modified version of equation 7, which - if given production data for different Hydrogen Sulphide inlet concentrations - could allow for the future investigation of the effect of H_2S in the process. The modified reaction rate equation is (eq. 11).

$$R'_{dep_1} = k'_1 \cdot p_{H_2S} \cdot p_{AlCl_3} \cdot p_{H_2O} \cdot p_{HCl}^{-1} \quad (mol \cdot m^{-2} \cdot s^{-1}) \tag{11}$$

4. Results

Since proprietary industrial production data are used for model validation, absolute thickness and deposition rate values cannot be presented. Therefore, only relative values are presented. Two main metrics are given, considering the predicted ($y_{prediction}$) and the actual (y_{actual}) deposition thickness values:

1. The relative error (RE), which is calculated by the following formula:

$$RE = \frac{y_{prediction} - y_{actual}}{y_{actual}} \tag{12}$$

2. The mean absolute percentage error (MAPE), which is calculated for each geometry by averaging the N absolute values (in our case, $N = 3$) of the relative error per reactor geometry.

$$MAPE = \frac{1}{N}\sum_{i=1}^{N} |\frac{y_{prediction,i} - y_{actual,i}}{y_{actual,i}}| \tag{13}$$

4.1. Parameter fitting and model validation

After conducting a mesh independence study for meshes consisting of 129195, 182609 and 287109 elements, a mesh of 129195 elements was used

for the discretization of the combined gas flow / α-Al_2O_3 deposition problem. This resulted in a problem consisting of about 10^6 degrees of freedom. Solution time was approximately 3.5 core hours on an 11th Gen Intel(R) Core(TM) i7-1185G7 processor. When compared with the resources required for the 2D, full reactor model ($5 \cdot 10^6$, 66 core hours solution time), an important difference in the required resources can be observed.

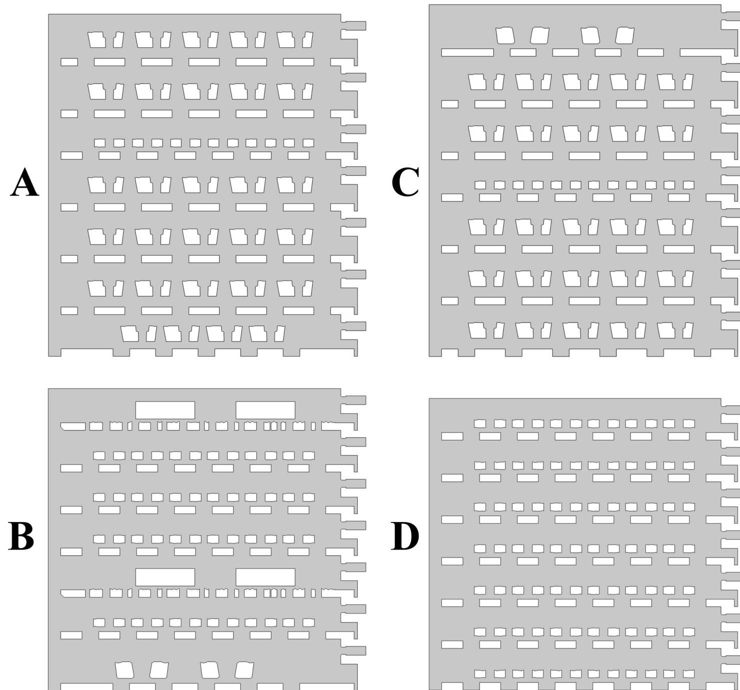

Figure 6: The four 7-disk geometries used in the CFD simulations. All cases are different parts of the same reactor.

An important challenge for this application is the fact that there are no CFD results reported in the literature. To our knowledge, this is the first attempt and therefore the model can only be validated using the available production data. For this reason, four different 7-disk parts of the same

reactor are simulated: Geometry A is used for fitting the kinetic parameters of the chemistry model; Geometries B, C, and D (Fig. 6) are used for the validation of the model in set-ups, i.e combinations of disks and inserts, representing different parts of the same reactor, where the flow and species concentration distributions are not expected to be the same as in Geometry A. The four geometries are determined by several factors, such as the shape and size of inserts to be coated and the geometry of the disks that carry each type of inserts (each insert has a specific disk geometry). The latter means that the perforations of the disks have a different diameter and the number of inserts in each disk is different, affecting in this way the overall surface area at each disk.

The kinetic parameters are adjusted so that the difference between the predicted and the production deposition thickness values is minimized. The comparison between the production and predicted thickness values is done in three different positions (cf. Fig. 5b): R_0 which is closest to the inlet, $R_{1/2}$ which is mid-distance between inlet and outlet and R, close to the outlet.

The first step towards fitting the kinetic parameters was choosing initial values. The initial value for the kinetic constant of the Water-gas-shift reaction was taken from the publication of Bustamante et al. (2004). For the surface reaction kinetic constants k_1 (eq.7) and k_2 (eq.8), the initial values were set to 0.001 $s \cdot mol/(kg \cdot m)$ and 10^{-6} $mol \cdot m^{-1.85} \cdot s^{-0.7} \cdot kg^{-0.15}$ respectively. These values led to a great underestimation of the coating thickness at all positions.

After trying different values for the kinetic parameters, it became clear that the reason for this severe underestimation was the value of the kinetic constant of the WGS reaction. This parameter was then fitted (as mentioned

in section 3.4) to achieve coating thickness predictions in the same order of magnitude as the available production data. An increase of this parameter led to higher coating thickness overall. By making a tenfold increase in the WGS pre-exponential factor, we obtain results comparable to the production data, however, the deposition thickness at the position closest to the inlet is overestimated (RE: 33.8% @ R_0, 7.7% @ $R_{1/2}$, 13.2% @ R).

The next step was to reduce the overestimation of the deposition thickness at the position closest to the inlet (R_0). By observing the results of the simulations for different values of k_1, it was clear that this overestimation could be mended by selecting a lower value of the parameter. Therefore, when setting $k_1 = 3 \cdot 10^{-5} s \cdot mol/(kg \cdot m)$ along with a nine-fold increase of the pre-exponential factor of the WGS reaction, slightly underestimating predictions are obtained (RE: -6.2% @ R_0, -4.2% @ $R_{1/2}$, -5.3% @ R).

After obtaining these results, the authors decided to make the transition from k_1 to k_1', trying to include in this way the concentration of H_2S into the α-Al_2O_3 deposition rate (via the proposed rate of eq. 11). Based on the average H_2S concentration inside the reactor and the value of k_1 that yielded the previous results, an initial value of $9 \cdot 10^{-7} s^3 \cdot mol/kg^2$ was set for k_1'. This led to underestimation of the coating thickness (RE: -23.8% @ R_0, -20.5% @ $R_{1/2}$, -21.0% @ R). Increasing k_1' to $1.1 \cdot 10^{-6} s^3 \cdot mol/kg^2$, only slightly amended this underestimation (RE: -20.6% @ R_0, -20.4% @ $R_{1/2}$, -20.8% @ R).

Having observed from previous simulation that an increase WGS reaction pre-exponential factor helps in reducing the underestimation of coating thickness at all positions, an eleven-fold increase was made. This yielded promising results (RE: -4.2% @ R_0, -3.4% @ $R_{1/2}$, -4.3% @ R). With some further fine-tuning, we ended up multiplying the pre-exponential factor of

1 the WGS reaction (k_{wgs}) by a factor of 11.25.

2 The derived kinetic parameter values shown in Table 1, lead to prediction
3 error of 2% at most in each one of the three positions (R_0, $R_{1/2}$ and R) in
4 Geometry A.

Table 1: The fitted kinetic constants used for the simulation of the α-Al_2O_3 deposition.

Parameter	Value	Units	Equation
k_{wgs}	$1.35 \cdot 10^{17}$	$m^{1.5} \cdot mol^{-0.5} \cdot s^{-1}$	9
k'_1	$1.1 \cdot 10^{-6}$	$s^3 \cdot mol \cdot kg^{-2}$	11
k_2	10^{-6}	$mol \cdot m^{-1.85} \cdot s^{-0.7} \cdot kg^{-0.15}$	8

5 The results, for Geometries B, C and D are presented in Fig. 7. Overall,
6 the proposed CFD model predicts the actual thickness values within a 4%
7 error (with the exception of the $R_{1/2}$ position in Geometry D which has
8 an error of 8%). In terms of the mean absolute error, during fitting it is
9 1.33% in Geometry A while the highest value is in Geometry D (4.33%).
10 For Geometries B and C, the mean absolute percentage error is 3.67% and
11 2.33% respectively (Fig. 7b).

12 *4.2. Investigation of the rate-limiting mechanism*

13 The CFD simulation, allows us to take a closer look at the actual con-
14 centration distributions of the reactants, namely of the precursor ($AlCl_3$)
15 and water, in the 4 geometries studied (cf. Fig. 6).

16 When considering the concentration of water (cf. Fig. 8), the CFD model
17 predicts almost uniform distribution above the inserts in the disk where the
18 coating thickness is predicted. Some regions of high water concentration are
19 predicted, however they are not located above the inserts. On the contrary,
20 the $AlCl_3$ concentration consistently appears to be higher closer to the inlet

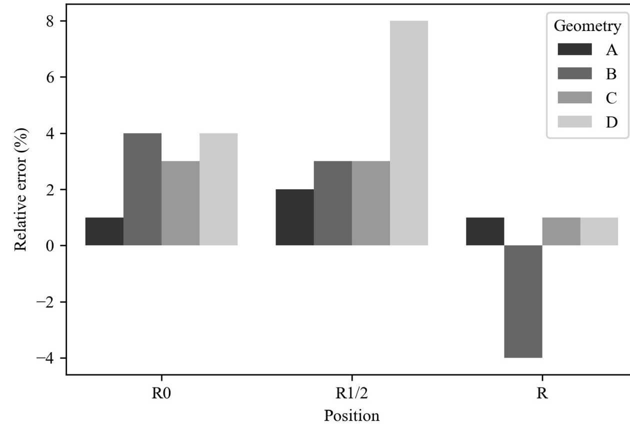

(a)

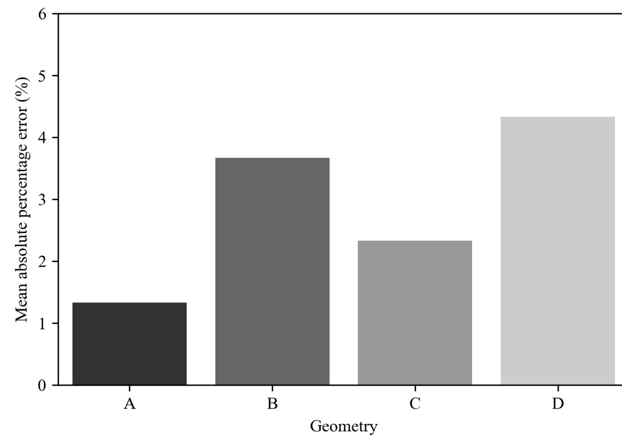

(b)

Figure 7: The developed model is tested for 4 distinct 7-disk geometries. The coating thickness predicted by CFD simulations is compared to production thickness values in three different positions (R_0, $R_{1/2}$ and R). Geometry A is used for calibration of the chemistry-enhanced CFD model, which is then tested in Geometries B, C and D. (a) Errors relative to the production data per geometry. (b) The mean absolute percentage error (MAPE) for each one of the four geometries. The highest error (observed for Geometry D) does not exceed 5%.

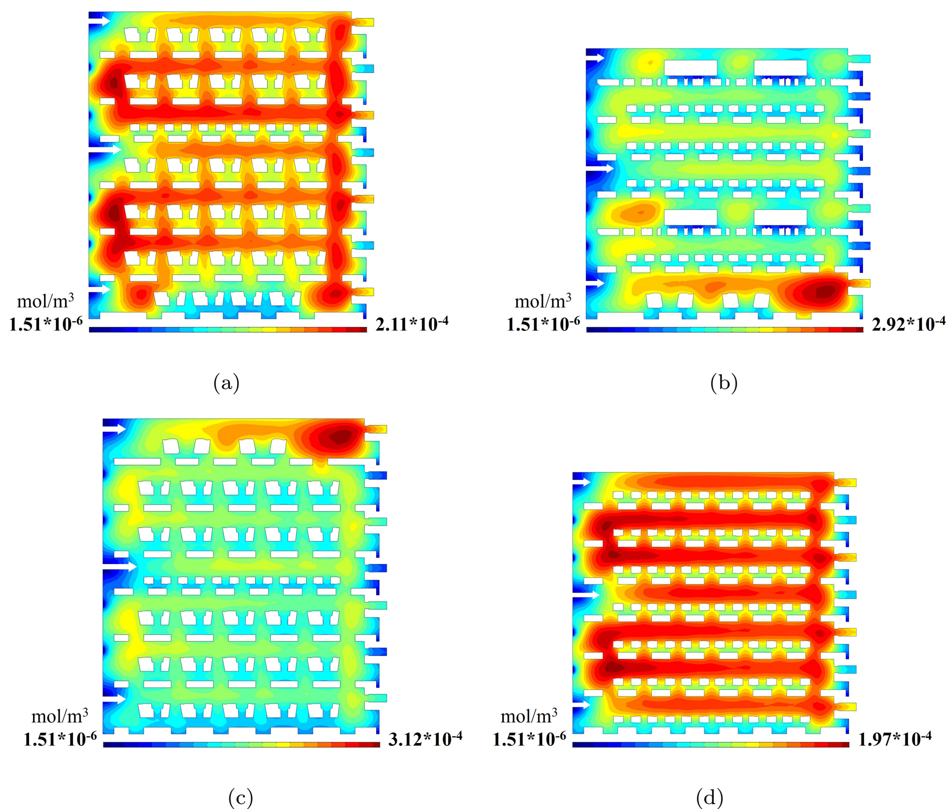

Figure 8: Contours of the concentration of H_2O for (a) Geometry A, (b) Geometry B, (c) Geometry C, (d) Geometry D. The white arrows indicate the velocity at each inlet. The CFD results suggest a mostly uniform concentration of water above the inserts.

of the reactor (cf. Fig. 9). This imbalance is not reflected in the thickness of the deposited material either in the simulations or, in fact, in the production data. This observation motivates further investigation into the balance between mass transfer (diffusion) and the reaction kinetics, that ultimately determines the rate-limiting step of the process.

Typically, this study requires altering the temperature and monitoring the change in the deposition rate. For increasing temperature the deposi-

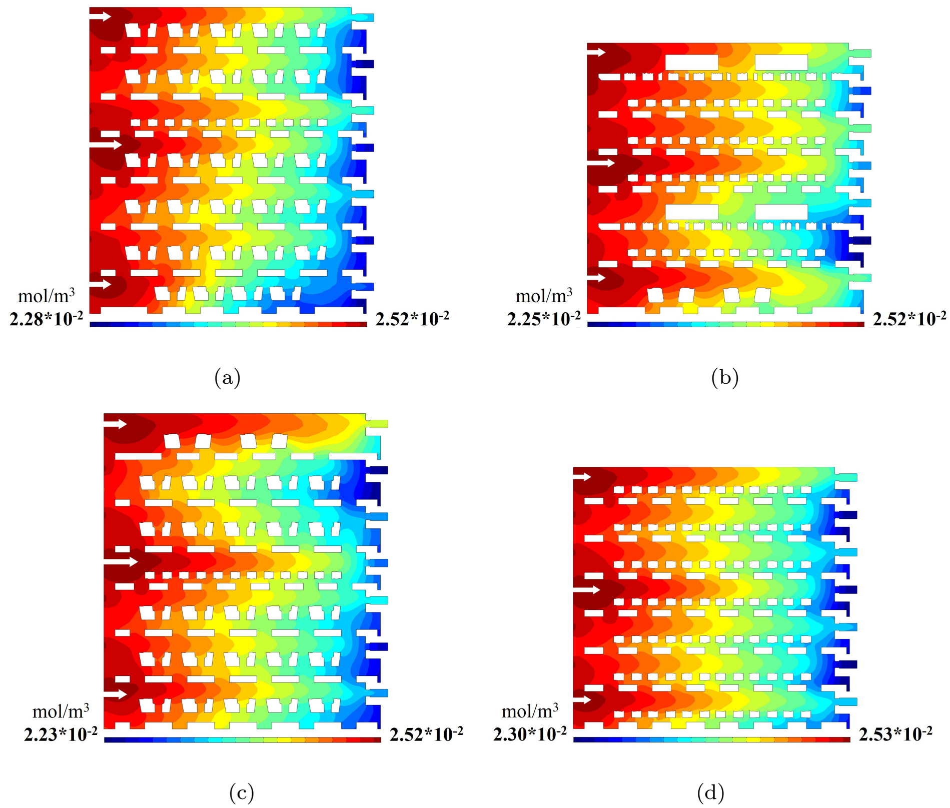

Figure 9: Contours of the concentration of $AlCl_3$ for (a) Geometry A, (b) Geometry B, (c) Geometry C, (d) Geometry D. The white arrows indicate the velocity at each inlet. The CFD results suggest highest precursor concentration close to the inlets.

1 tion rate also increases following a linear trend, which is an indication that
2 the reaction rate is the limiting step that determines the overall deposition
3 rate. Past a certain temperature, the deposition rate becomes insensitive to
4 further increase of the temperature, which is a sign that the rate of diffusion
5 of the species on the surface determines the overall deposition rate. This
6 process is typically described in a so-called Arrhenius plot, i.e. the plot of
7 the deposition rate versus the inverse of temperature (Psarellis et al., 2018).

8 In the application studied here, where the data are derived from the

1 production process at a single temperature (1005 °C), it is not possible to
2 derive an Arrhenius plot based on which to define whether the process is
3 kinetics or diffusion limited. Instead, it is still possible to gain insight into
4 this balance with the proposed CFD model by means of studying the effect
5 of the precursor mass fraction on the coating thickness: two computational
6 experiments are performed, based on Geometry A, one with significantly
7 increased precursor mole fraction at the inlet (by 25%), the second with
8 significantly decreased (by 25%).

9 If the process were diffusion limited, then the reactions would be very fast
10 and as soon as the precursor molecules reach the surface, they would react
11 forming more α-Al_2O_3 on the surface. Therefore an increase/decrease is
12 expected as an outcome when the $AlCl_3$ mole fraction is increased/decreased
13 respectively. On the contrary, if the deposition rate is affected to a negligible
14 extent, then this would be a valid indication that the process is in the
15 kinetics-limited regime. This comparison is shown in Table 2 where the
16 "original" experiment, corresponding to the process conditions in Geometry
17 A, is compared to the CFD results obtained in the same Geometry and
18 conditions with different mole fractions of precursor at the inlet.

Table 2: Difference in the deposition rate for different precursor concentrations at the inlet - Geometry A. Values are relative to the original simulation.

Position	$\mathbf{R_0}$	$\mathbf{R_{1/2}}$	**R**	**$AlCl_3$ inlet mol. frac.**
Relative difference (%)	4.5	-0.4	-0.1	1.25×Original
	-7.3	-0.3	-0.1	0.75×Original

19 The results indicate that the change in the $AlCl_3$ mole fraction leads
20 to negligible fluctuations in the calculated deposition rate for the insert at

1 the $R_{1/2}$ and R position, which corroborates the hypothesis that the process
2 is in a kinetics-limited regime. Slight discrepancies appear in the insert
3 at the R_0 position. Specifically, for the experiment with 25% increased
4 precursor mole fraction, there is a 4.5% increase in the deposition rate for
5 the insert at R_0, when compared to the original run. For the experiments
6 with a precursor mole fraction of 25% less than the original, the calculated
7 α-Al_2O_3 deposition rates for the insert at R_0 are 7.3% less than the original
8 experiment. This finding is not contrary to the hypothesis of a kinetics-
9 limited regime and can be explained by considering the concentration of the
10 other reactant, water, in the region above the inserts on interest, summarized
11 in Table 3. In the case of increased $AlCl_3$ mole fraction, the concentration
12 of water is higher above the insert in the R_0 position, leading to higher
13 deposition thickness. In contrast, in the case of decreased precursor mole
14 fraction, water concentration is lower above the insert in the R_0 position,
15 leading to decreased deposition rate. Overall though it could be argued that
16 this discrepancy in the R_0 position of 4.5% increase and 7.3% decrease in
17 the deposition rate can still be considered minor, taking into consideration
18 that the alteration to the precursor concentration is by 25%.

Table 3: Average H_2O concentrations above the inserts of interest for different inlet precursor concentrations - Geometry A.

Position	$\mathbf{R_0}$	$\mathbf{R_{1/2}}$	**R**	**$\mathbf{AlCl_3}$ inlet mol. frac.**
H_2O conc. (10^{-4}mol/m^3)	1.92	1.95	1.87	Original
	1.66	1.59	1.52	1.25·Original
	2.30	2.53	2.47	0.75·Original

5. Conclusions

This work presents an efficient tool for computational analysis of an industrial-scale CVD reactor used for the coating of cutting tool inserts. The proposed CFD model addresses three significant challenges not only in Chemical Vapor Deposition but also in other processes where chemistry and transport phenomena co-exist: (i) Complex geometries, (ii) Complicated networks of chemical reaction which are not completely known, (iii) Competition between the physical and chemical mechanisms, something that ultimately defines the rate of the overall process.

We demonstrated how this computer-aided approach can predict the thickness of the deposited film with noteworthy accuracy (with a 5% average error). To do so, we implemented a chemistry model that with one homogeneous and one heterogeneous reaction, for the sake of efficiency, which nevertheless takes into account the concentration of hydrogen sulphide. The latter is generally understood to act as a catalyst but to this date there is no consensus on the actual mechanism.

Despite the simplifications introduced for the sake of economizing on the computational effort, the proposed model is still able to illuminate important aspects of the interplay of physical phenomena (mass transport through diffusion) and chemical reaction rates. Results for higher and lower precursor concentrations in the inlet, point to the fact that the process is in the kinetics-limited regime, where the overall deposition rate in determined by the relatively slow reaction rate. Although further investigation is required to determine this fact with certainty, the input of the proposed model is still a useful "hint" to the direction that should be followed experimentally.

Acknowledgements

The authors would like to thank Dr. G.P. Gakis and Dr. I.G. Aviziotis for their valuable input and our fruitful discussions at the initial stages of this work. P.P. and E.D.K. acknowledge financial support by the Fonds National de la Recherche (FNR) Luxembourg (BRIDGE grant HybridSim-CVD). E.D.K. is supported by the EU under a MSCA Individual Fellowship. S.P.A.B received funding from the European Union's Horizon 2020 research and innovation program under grant agreement No 811099 TWINNING Project DRIVEN for the University of Luxembourg. T.J.M acknowledges financial support by the University of Houston through the William A. Brookshire Endowed Chair.

References

Ban, W., Kwon, S., Nam, J., Yang, J., Jang, S., Jung, D., 2017. Al2O3 thin films prepared by plasma-enhanced chemical vapor deposition of dimethylaluminum isopropoxide. Thin Solid Films 641, 47–52. doi:10.1016/j.tsf.2017.02.007.

Bar-Hen, M., Etsion, I., 2017. Experimental study of the effect of coating thickness and substrate roughness on tool wear during turning. Tribology International 110, 341–347. doi:10.1016/j.triboint.2016.11.011.

Barua, H., Povitsky, A., 2020. Numerical model of carbon chemical vapor deposition at internal surfaces. Vacuum 175, 109234. doi:10.1016/j.vacuum.2020.109234.

Blomqvist, A., Århammar, C., Pedersen, H., Silvearv, F., Norgren, S., Ahuja, R., 2011. Understanding the catalytic effects of H2S on CVD-

growth of α-alumina: Thermodynamic gas-phase simulations and density functional theory. Surface and Coatings Technology 206, 1771–1779. doi:10.1016/j.surfcoat.2011.09.018.

Bustamante, F., Enick, R.M., Cugini, A., Killmeyer, R.P., Howard, B.H., Rothenberger, K.S., Ciocco, M.V., Morreale, B.D., Chattopadhyay, S., Shi, S., 2004. High-temperature kinetics of the homogeneous reverse water-gas shift reaction. AIChE Journal 50, 1028–1041. doi:10.1002/aic.10099.

Catoire, L., Swihart, M.T., 2002. High-Temperature Kinetics of AlCl3 Decomposition in the Presence of Additives for Chemical Vapor Deposition. Journal of The Electrochemical Society 149, C261. doi:10.1149/1.1467366.

Cheimarios, N., Kavousanakis, M., Kokkoris, G., Boudouvis, A., 2019. Beware of symmetry breaking and periodic flow regimes in axisymmetric CVD reactor setups. Computers & Chemical Engineering 124, 124–132. doi:10.1016/j.compchemeng.2019.02.005.

Cheimarios, N., Koronaki, E.D., Boudouvis, A.G., 2012. Illuminating nonlinear dependence of film deposition rate in a CVD reactor on operating conditions. Chemical Engineering Journal 181–182, 516–523. doi:10.1016/j.cej.2011.11.008.

Cho, J., Mountziaris, T.J., 2013. Onset of flow recirculation in vertical rotating-disc chemical vapor deposition reactors. AIChE Journal 59, 3530–3538. doi:10.1002/aic.14179.

Creighton, J.R., Parmeter, J.E., 1993. Metal CVD for microelectronic ap-

plications: An examination of surface chemistry and kinetics. Critical Reviews in Solid State and Materials Sciences 18, 175–237. doi:10.1080/10408439308242560.

Etchepare, P., Vergnes, H., Samélor, D., Sadowski, D., Brasme, C., Caussat, B., Vahlas, C., 2014. Amorphous Alumina Coatings on Glass Bottles Using Direct Liquid Injection MOCVD for Packaging Applications, in: 13th International Ceramics Congress, Part of CIMTEC 2014, pp. 117–122. doi:10.4028/www.scientific.net/AST.91.117.

Gakis, G., Koronaki, E., Boudouvis, A., 2015. Numerical investigation of multiple stationary and time-periodic flow regimes in vertical rotating disc CVD reactors. Journal of Crystal Growth 432, 152–159. doi:10.1016/j.jcrysgro.2015.09.026.

Gassner, M., Schalk, N., Tkadletz, M., Czettl, C., Mitterer, C., 2019. Thermal crack network on CVD TiCN/α-Al2O3 coated cemented carbide cutting tools. International Journal of Refractory Metals and Hard Materials 81, 1–6. doi:10.1016/j.ijrmhm.2019.02.006.

Gassner, M., Schalk, N., Tkadletz, M., Pohler, M., Czettl, C., Mitterer, C., 2018. Influence of cutting speed and workpiece material on the wear mechanisms of CVD TiCN/α-Al2O3 coated cutting inserts during turning. Wear 398–399, 90–98. doi:10.1016/j.wear.2017.11.019.

Gkinis, P., Aviziotis, I., Koronaki, E., Gakis, G., Boudouvis, A., 2017. The effects of flow multiplicity on GaN deposition in a rotating disk CVD reactor. Journal of Crystal Growth 458, 140–148. doi:10.1016/j.jcrysgro.2016.10.065.

1 Hochauer, D., Mitterer, C., Penoy, M., Puchner, S., Michotte, C., Martinz,
2 H., Hutter, H., Kathrein, M., 2012. Carbon doped α-Al2O3 coatings
3 grown by chemical vapor deposition. Surface and Coatings Technology
4 206, 4771–4777. doi:10.1016/j.surfcoat.2012.03.059.

5 Jensen, K.F., Einset, E.O., Fotiadis, D.I., 1991. Flow phenomena in
6 chemical vapor deposition of thin films. Annual Review of Fluid
7 Mechanics 23, 197–232. doi:10.1146/annurev.fl.23.010191.001213,
8 arXiv:https://doi.org/10.1146/annurev.fl.23.010191.001213.

9 Kathrein, M., Schintlmeister, W., Wallgram, W., Schleinkofer, U.,
10 2003. Doped CVD Al2O3 coatings for high performance cutting tools.
11 Surface and Coatings Technology 163–164, 181–188. doi:10.1016/
12 s0257-8972(02)00483-8.

13 Keiski, R.L., Salmi, T., Niemistö, P., Ainassaari, J., Pohjola, V.J., 1996.
14 Stationary and transient kinetics of the high temperature water-gas shift
15 reaction. Applied Catalysis A: General 137, 349–370. doi:10.1016/
16 0926-860x(95)00315-0.

17 Koronaki, E.D., Gakis, G.P., Cheimarios, N., Boudouvis, A.G., 2016. Ef-
18 ficient tracing and stability analysis of multiple stationary and periodic
19 states with exploitation of commercial CFD software. Chemical Engineer-
20 ing Science 150, 26–34. doi:10.1016/j.ces.2016.04.043.

21 Mitrovic, B., Gurary, A., Kadinski, L., 2006a. On the flow stability in
22 vertical rotating disc MOCVD reactors under a wide range of process
23 parameters. Journal of Crystal Growth 287, 656–663. doi:10.1016/j.
24 jcrysgro.2005.10.131.

Mitrovic, B., Gurary, A., Quinn, W., 2007. Process conditions optimization for the maximum deposition rate and uniformity in vertical rotating disc MOCVD reactors based on CFD modeling. Journal of Crystal Growth 303, 323–329. doi:10.1016/j.jcrysgro.2006.11.247.

Mitrovic, B., Parekh, A., Ramer, J., Merai, V., Armour, E., Kadinski, L., Gurary, A., 2006b. Reactor design optimization based on 3D modeling of nitrides deposition in MOCVD vertical rotating disc reactors. Journal of Crystal Growth 289, 708–714. doi:10.1016/j.jcrysgro.2005.12.107.

Munro, R.G., 1997. Evaluated Material Properties for a Sintered alpha-Alumina. Journal of the American Ceramic Society 80, 1919–1928. doi:10.1111/j.1151-2916.1997.tb03074.x.

Oshika, T., Nishiyama, A., Nakaso, K., Shimada, M., Okuyama, K., 1999. Unveiling the magic of H $_2$ S on the CVD-Al $_2$ O $_3$ coating. Le Journal de Physique IV 09, Pr8–877–Pr8–883. doi:10.1051/jp4:19998110.

Ozaydin-Ince, G., Coclite, A.M., Gleason, K.K., 2011. CVD of polymeric thin films: Applications in sensors, biotechnology, microelectronics/organic electronics, microfluidics, MEMS, composites and membranes. Reports on Progress in Physics 75, 016501. doi:10.1088/0034-4885/75/1/016501.

Paseuth, A., Fukui, H., Yamagata, K., 2016. Improvement of mechanical properties and cutting performance of modified MT-TiCxN1-x coating by moderate temperature chemical vapor deposition. Surface and Coatings Technology 291, 54–61. doi:10.1016/j.surfcoat.2016.02.023.

Prengel, H., Pfouts, W., Santhanam, A., 1998. State of the art in hard

1 coatings for carbide cutting tools. Surface and Coatings Technology 102, 183–190. doi:10.1016/S0257-8972(96)03061-7.

Psarellis, G.M., Aviziotis, I.G., Duguet, T., Vahlas, C., Koronaki, E.D., Boudouvis, A.G., 2018. Investigation of reaction mechanisms in the chemical vapor deposition of al from DMEAA. Chemical Engineering Science 177, 464–470. doi:10.1016/j.ces.2017.12.006.

Quinto, D., 1996. Technology perspective on CVD and PVD coated metal-cutting tools. International Journal of Refractory Metals and Hard Materials 14, 7–20. doi:10.1016/0263-4368(96)83413-5.

Ruppi, S., 2020. Influence of Process Conditions on the Growth and Texture of CVD Alpha-Alumina. Coatings 10, 158. doi:10.3390/coatings10020158.

Schierling, M., Zimmermann, E., Neuschütz, D., 1999. Deposition kinetics of Al_2O_3 from $AlCl_3$-CO_2-H_2-HCl gas mixtures by thermal CVD in a hot-wall reactor. Le Journal de Physique IV 09, Pr8–85–Pr8–91. doi:10.1051/jp4:1999811.

Spencer, R., Gkinis, P., Koronaki, E., Gerogiorgis, D., Bordas, S., Boudouvis, A., 2021. Investigation of the chemical vapor deposition of Cu from copper amidinate through data driven efficient CFD modelling. Computers & Chemical Engineering 149, 107289. doi:10.1016/j.compchemeng.2021.107289.

Stylianou, R., Tkadletz, M., Schalk, N., Penoy, M., Czettl, C., Mitterer, C., 2019. Effects of reference materials on texture coefficients determined for

a CVD α-Al2O3 coating. Surface and Coatings Technology 359, 314–322. doi:10.1016/j.surfcoat.2018.12.095.

Tan, P., Müller, J., Neuschütz, D., 2005. Gas-Phase Kinetic Modeling of the AlCl3 Decomposition in the AlCl3-CO2-H2-HCl System for a Hot-Wall CVD Reactor. Journal of The Electrochemical Society 152, C288. doi:10.1149/1.1883236.

Theodoropoulos, C., Ingle, N., Mountziaris, T., 1997. Computational studies of the transient behavior of horizontal MOVPE reactors. Journal of Crystal Growth 170, 72–76. doi:10.1016/s0022-0248(96)00637-9.

Theodoropoulos, C., Mountziaris, T., Moffat, H., Han, J., 2000. Design of gas inlets for the growth of gallium nitride by metalorganic vapor phase epitaxy. Journal of Crystal Growth 217, 65–81. doi:10.1016/s0022-0248(00)00402-4.

Tingey, G.L., 1966. Kinetics of the Water—Gas Equilibrium Reaction. I. The Reaction of Carbon Dioxide with Hydrogen. The Journal of Physical Chemistry 70, 1406–1412. doi:10.1021/j100877a011.

van Santen, H., Kleijn, C.R., van den Akker, H.E.A., 2001. On multiple stability of mixed-convection flows in a chemical vapor deposition reactor. International Journal of Heat and Mass Transfer 44, 659–672. doi:10.1016/s0017-9310(00)00121-6.

Yousefian, P., Pimputkar, S., 2021. Computational fluid dynamics modeling of a new high-pressure chemical vapor deposition reactor design. Journal of Crystal Growth 566–567, 126155. doi:10.1016/j.jcrysgro.2021.126155.

Zou, S., Xiao, J., Wu, V., Chen, X.D., 2021. Analyzing industrial CVD reactors using a porous media approach. Chemical Engineering Journal 415, 129038. doi:10.1016/j.cej.2021.129038.